Ultrahigh tensile strength of water confined in carbon nanotubes: Mechanism and relevance to long-distance water transport in tall trees

Si-Qi Yu, Xiao-Yan Zhou,* and Hang-Jun Lu†
Department of Physics, Zhejiang Normal University, Jinhua 321004, China

(Received 4 February 2026; accepted 22 June 2026; published 3 November 2026)

Molecular dynamics simulations are employed to investigate the tensile properties of water confined in carbon nanotubes (CNTs) with varying diameters, where CNTs serve as a prototype for xylem vessels critical to long-distance water transport in tall trees. Our results reveal that nanoconfined water exhibits unexpectedly ultrahigh tensile strength (∼126 MPa), which is significantly higher than that of glass (∼33 MPa). Meanwhile, the tensile strength of confined water is highly dependent on the nanotube diameter. The underlying mechanism for this unique tensile behavior is attributed to the synergistic effect of hydrogen bonding and nanoscale confinement. This work provides key insights into understanding the mechanism of water transport from roots to the canopy in tall trees.

DOI: 10.1103/sjsb-289q

I. INTRODUCTION

Water under nanoconfinement exhibits a variety of structural, thermodynamic, and dynamic anomalies that differ markedly from its bulk behavior [1–11]. These effects are of fundamental interest in understanding water-related processes in biological, geological, and nanofluidic systems [12–17]. Molecular simulations have revealed that spatial confinement can induce novel hydrogen-bond networks, reduced entropy, and unconventional ice phases, such as two-dimensional layered ice and polygonal ice nanotubes [18,19]. Such findings have stimulated extensive investigations into confined water, both theoretically and experimentally [8,20–31]. Beyond equilibrium structures, the transport properties of confined water have attracted significant attention [32–35]. Due to reduced interfacial friction and enhanced slip, water flow in carbon nanotubes can exceed classical predictions by orders of magnitude [36]. Similar frictionless behavior has been observed in two-dimensional channels formed by graphene-based membranes [37–39]. These transport anomalies are closely linked to confinement-induced changes in water structure and dynamics [40–42].

While extensive efforts have been devoted to understanding the structure and transport behavior of confined water, its mechanical response—particularly under tensile conditions—remains far less explored. This knowledge gap is notably relevant to the long-distance water transport mechanism in plants, a topic that has captivated plant scientists for over a century. There is considerable interest in unraveling how water moves from the roots to the canopy of tall trees, especially given that the tallest tree on earth today exceeds 110 m in height. According to physical principles, atmospheric pressure can only support a water column of approximately 10.3 m, making it theoretically impossible to lift water beyond this height solely through pressure reduction at the tree canopy. To address this paradox, the cohesion-tension theory proposes that long-distance water transport in plants relies on the stability of continuous water columns under large negative pressures [43]. However, the existence and magnitude of such high tensions (up to tens of MPa) remain controversial, partly due to experimental limitations and discrepancies in direct pressure measurements [44,45]. These unresolved questions underscore the critical need for atomistic-level investigations into confined water columns under tension. In particular, the influence of nanoscale confinement on the tensile strength of water columns—a key factor in maintaining column stability—has not yet been fully elucidated.

Plants are composed of nano- to microscale porous structures extending from roots to leaves, through which long-distance water transport is stably maintained [46]. While the macroscopic xylem vessel lumens typically range from 10 to 500 μm, the critical nanoscale pathways for water tension and stabilization—namely nanopores within xylem pit membranes and mesophyll cell walls—are widely documented to be 1–3 nm [47].

In this work, we employ molecular dynamics simulations to investigate the tensile behavior of water columns confined within carbon nanotubes (CNTs) of various diameters. By characterizing the critical tension and failure dynamics under different confinement conditions, we find that these nanoconfined water columns can sustain remarkably high tensile stresses, with the critical tension reaching a maximum of approximately 126 MPa at a tube radius of around 1.35 nm. Notably, the critical tension exhibits a nonlinear, nonmonotonic dependence on tube radius—a distinctive trend closely tied to the structural properties and fracture mechanisms of the confined water. Moreover, this ultrahigh tensile strength far exceeds that of bulk glass (∼33 MPa), highlighting the exceptional mechanical performance of water under nanoscale confinement.

*Contact author: zxylu@zjnu.cn
†Contact author: zjlhjun@zjnu.cn

 ©2026 American Physical Society

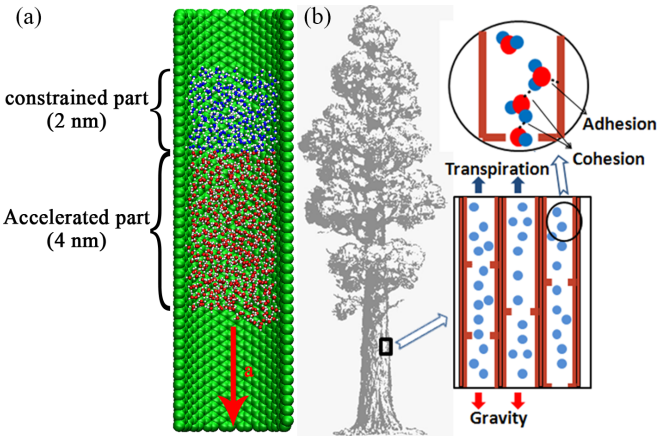


FIG. 1. (a) Typical simulation system, where a single-walled CNT(20,20) with a length of 10 nm is aligned along the z axis and contains a 6 nm water column. The water column is divided into two groups: the upper 2 nm is defined as the restrained group (blue water molecules) and the lower 4 nm is defined as the pulled group. An acceleration along the negative z axis is applied to the pulled group to simulate a downward stretching force. (b) Schematic illustration of water transport mechanisms in plants. In xylem vessels, water is subjected to gravitational force and is transported upward under transpiration pull. The cohesion among water molecules and the adhesion between water molecules and the vessel walls maintain the continuity of the water column, preventing it from breaking.

II. METHODS

To investigate the tensile behavior of confined water columns and their underlying microscopic mechanisms, we perform molecular dynamics simulations using a series CNT (n, n), with radii ranging from 0.678 to 2.708 nm ($n = 10$–40). A typical simulation setup is illustrated in Fig. 1(a), where a 10-nm-long CNT (20,20) with a radius of 1.35 nm is aligned along the z axis and kept fixed throughout the simulation. A water column of around 6 nm in length, consisting of 795 water molecules, is confined inside the CNT. The remaining space inside the nanotube is vacuum. To evaluate the maximum tensile stress the confined water can sustain, the water column is divided into two groups. The upper 2 nm segment, defined as the restrained group, is subjected to position restraints on the oxygen atoms along the z axis via a harmonic potential with a spring constant of $k = 1000\ \mathrm{kJ\,mol^{-1}nm^{-2}}$. The lower 4 nm segment, defined as the pulled group, is subjected to a constant acceleration a along the negative z direction, simulating tensile loading.

The tension of the water column inside the carbon nanotube was generated by applying an acceleration to the water molecules. A total external force acts on the stretching group of $F = Nma$, where N is the total number of water molecules in the stretching group and m is the mass of a water molecule.

The tensile stress of the water column was calculated by dividing the total external force by the effective cross-sectional area (A_{eff}). The effective cross-sectional area was defined as the inner cross-sectional area of the carbon nanotube excluding the region occupied by the van der Waals radius of the carbon atoms. The tensile stress of the confined water column can therefore be expressed as $\sigma = \frac{F}{A_{\mathrm{eff}}}$.

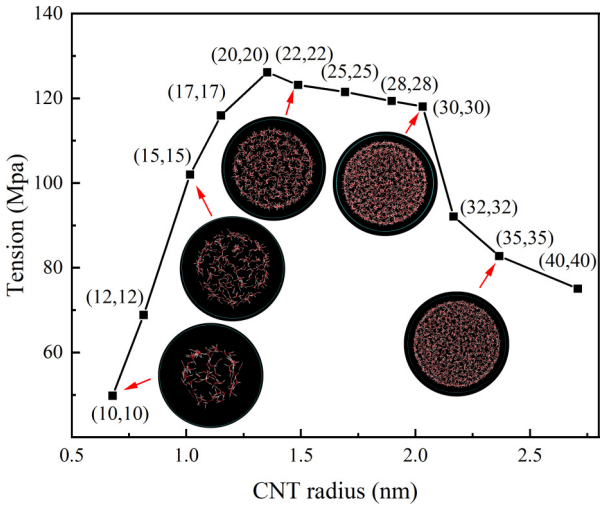


FIG. 2. Maximum negative pressure (tension) of the water confined within carbon nanotubes as a function of the tube radius. The insets show snapshots of the cross-sectional distributions of water molecules in the typical nanotubes indicated by the arrows.

All simulations are performed using GROMACS 2019.4 under the *NVT* ensemble. CNTs were parametrized using the OPLS-AA all-atom force field. Water molecules were modeled using TIP4P. The Lennard-Jones parameters between unlike atom types were determined using the Lorentz-Berthelot combining rules. The temperature is maintained at 300 K using the V-rescale thermostat with a coupling time constant of $\tau = 0.1$ ps. Long-range electrostatics are handled by the particle-mesh Ewald (PME) method. Periodic boundary conditions are imposed in all three directions and the time step is set to 1.0 fs. The initial systems are constructed using Packmol by filling the CNT interiors with water molecules. After energy minimization using the steepest descent algorithm to remove bad contacts, a 30 ns *NVT* equilibration is performed to obtain a stable water column with an axial length of approximately 6 nm. Subsequently, nonequilibrium simulations are carried out by gradually increasing the acceleration applied to the pulled group with a step size of $0.001\ \mathrm{nm\,ps^{-2}}$ until the water column fractures. Each simulation at a given acceleration lasts for 10 ns. The critical acceleration a_c is defined as the acceleration at which a rupture occurs. To determine a_c more accurately, additional simulations are performed within the range $a_c - \delta < a < a_c$, each lasting 100 ns, and multiple runs are conducted to reduce statistical fluctuations.

The carbon nanotubes were not fully filled with water molecules and both ends were left empty (vacant). Therefore, during equilibration at 300 K, the pressure of water remained nearly constant.

III. RESULTS AND DISCUSSION

The maximum negative pressure sustainable by water columns inside CNTs is shown in Fig. 2. Surprisingly, the confined water exhibits exceptionally high tensile strength inside single-walled CNTs, with critical pressures ranging from 43 MPa to 126 MPa within the studied radius range (0.678 to 2.708 nm), comparable to the tensile strength of glass.

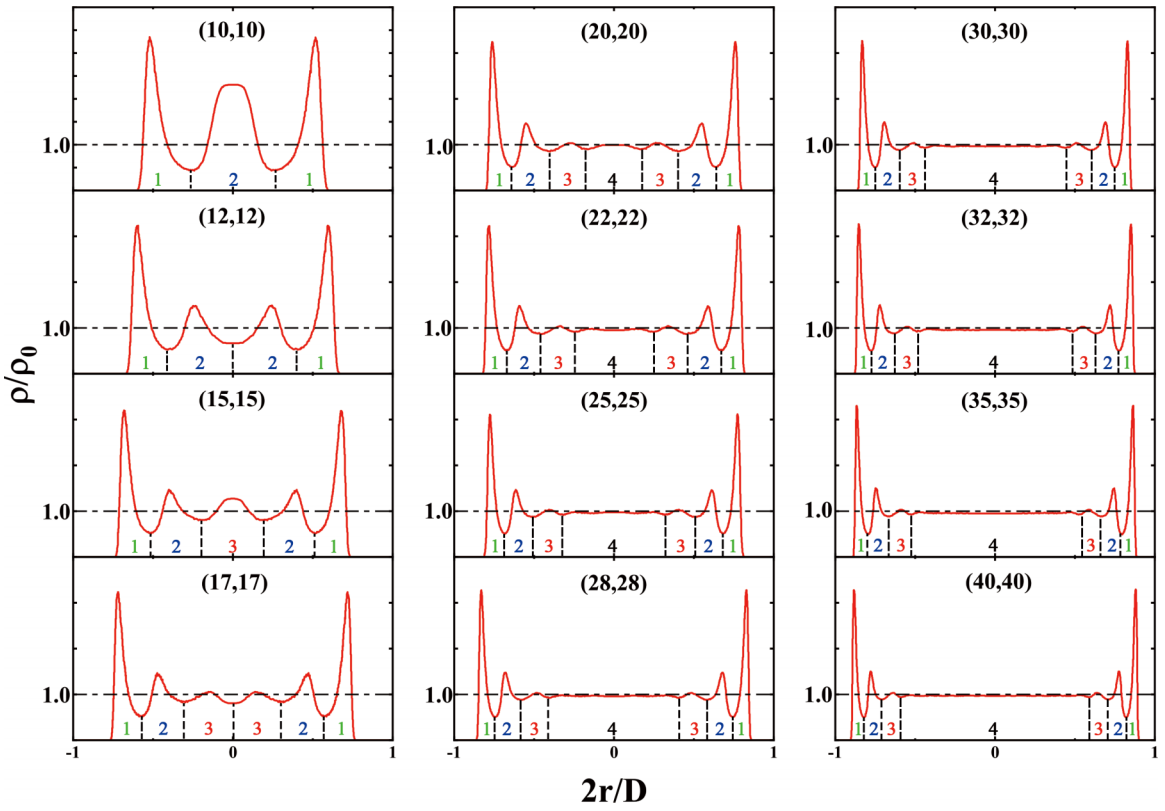


FIG. 3. Water density as a function of the radial distance toward the wall from the center of the tube at $r = 0$ nm.

Moreover, the tensile strength is found to be strongly dependent on the CNT radius. As the CNT size increases from (10,10) to (20,20), corresponding to a radius range of 0.678–1.353 nm, the maximum sustainable negative pressure increases rapidly from 43 MPa to 126 MPa. Interestingly, further increasing the CNT radius leads to a gradual decrease in the tensile strength. However, when the CNT radius is increased by only about 0.135 nm to that of a (32,32) CNT, the tensile strength drops significantly to around 92 MPa. As the CNT radius continues to increase, the tensile strength of the confined water columns shows a further decreasing trend. Our results shown in Fig. 2 demonstrate the rationality of a fascinating phenomenon: in nanoscale channels (nanopores, <2 nm) within plant cell walls, water—though normally susceptible to rupture under tensile stress—behaves as a robust, continuous liquid. This unique behavior is essential for transpiration, enabling water columns to withstand intense negative pressures (tension) and ascend from roots to aerial tissues, a process critical to sustaining plant life. In stark contrast, bulk water exhibits markedly lower tensile strength and cannot support such tension.

To elucidate the intrinsic mechanism governing the correlation between the tensile strength of the confined water column and the CNT radius, we analyzed the radial density distribution of water molecules within each nanotube, as illustrated in Fig. 3. The radial density function $\rho(r)$ was calculated by partitioning the confined water domain into a series of coaxial cylindrical shells along the radial direction of the CNT. For comparative purposes, the density function $\rho(r)$ was normalized against the density of bulk water under standard conditions ($\rho_0 = 1.0$ g/cm^3).

As shown in Fig. 3, water confined inside CNTs exhibits an obvious layering structure. Due to the van der Waals interactions between the water molecules and the CNT walls, a sharp density peak appears near the nanotube wall, with a width approximately equal to the size of a water molecule (∼0.34 nm), indicating a highly ordered single-layer arrangement in this region. For clarity, the confined water was delineated into distinct layers based on the radial density distribution—designated as the first, second, third, and fourth layers sequentially from the CNT wall toward the tube center (see Fig. 3).

For large-diameter CNTs ($d > 2.7$ nm), the first 1–3 molecular layers adjacent to the tube wall constitute the so-called interfacial water, which possesses a distinct structure that deviates markedly from that of bulk water. By contrast, water molecules beyond this interfacial region exhibit bulk-like characteristics. As shown in Fig. 3, water density gradually converges to bulk-water values beyond the third hydration layer, with no pronounced further density layering observed. Accordingly, our water-layer classification is defined solely based on the density distribution. It has been reported that, above four or five layers, the water gradually loses memory of the CNT wall and tends to acquire again the bulk water structure [48,49].

Notably, as the CNT radius increases, the number of discernible ordered water layers rises correspondingly and the tensile strength of the confined water column displays a positive correlation with the layer count. Specifically, when the radius reaches 1.353 nm—corresponding to a (20,20) CNT—the maximum number of water layers (four) is observed and the tensile strength of the confined water column peaks at

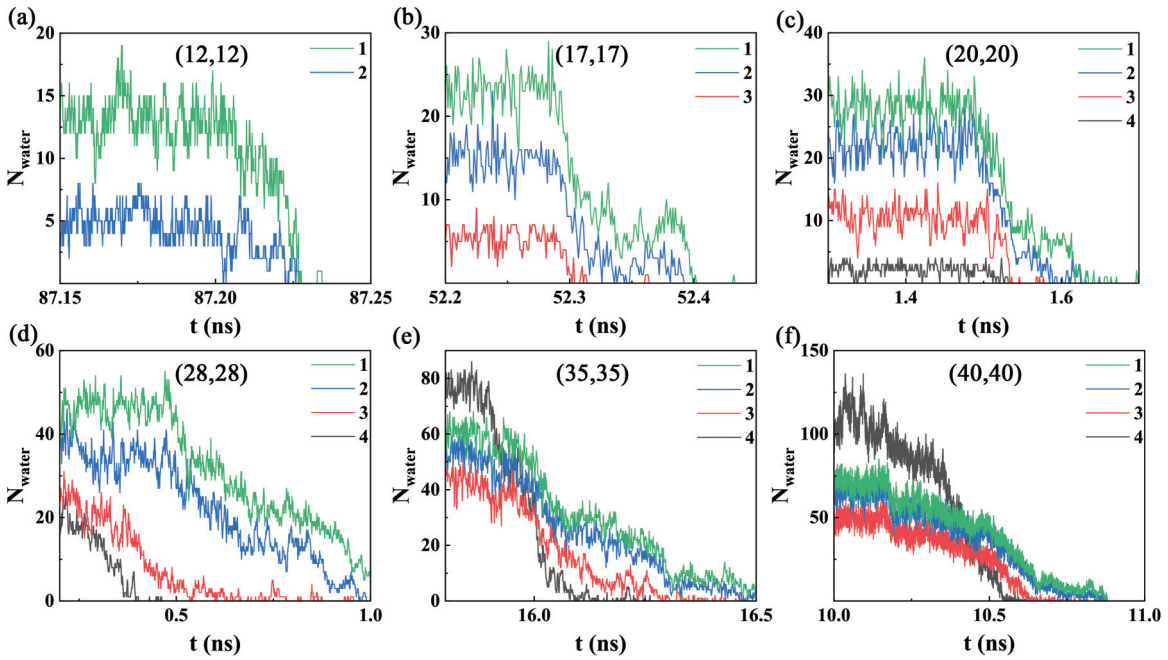


FIG. 4. Fracture process of water columns confined in CNTs with different diameters. The number of water molecules in each radial layer within the fracture region (1 nm along the z axis) is tracked as a function of time during rupture.

126 MPa. A further increase in CNT radius induces the expansion of the innermost (fourth) water layer, accompanied by a subsequent decline in tensile strength. In fact, when the CNT radius exceeds 1.353 nm, the fourth water layer no longer exists as a distinct single layer. These findings collectively demonstrate that the tensile strength of the confined water column is tightly correlated with the structural distribution of water molecules within the nanotube.

To understand the relationship between the tensile strength of confined water and the layered structure formed inside nanotubes, it is essential to first clarify the fracture mode of the water column. To this end, the fracture processes of water columns in CNTs of various diameters were systematically examined. During each fracture event, the number of water molecules in each defined radial layer within a 1 nm segment along the axial (z) direction centered at the rupture site was tracked over time. The results are presented in Fig. 4. For CNTs with $r \leqslant 1.353$ nm, such as the (12,12), (17,17), and (20,20) CNTs, the number of water molecules in all layers begins to decrease almost simultaneously during fracture, indicating a collective rupture of all layers under tension. This simultaneous failure suggests that the addition of more water layers significantly increases the required tensile stress to initiate rupture, providing a mechanistic explanation for the observed increase in tensile strength with increasing layer number. In contrast, when the CNT radius exceeds 1.353 nm, although the number of water layers no longer increases, the inner region of the confined water expands. In this case, a sequential rupture pattern is observed: in the (28,28) CNT, the third and fourth water layers begin to fail first, with the first and second layers following only after a noticeable delay. Similarly, in the (35,35) CNT, the rupture is initiated in the center (fourth) layer, followed by the outer layers. This inside-out fracture mode of confined water is in stark contrast to the fracture behavior of the bulk water column, in which rupture characteristically originates from the outer surface. It further diverges from the necking phenomenon that occurs in solid metal nanowires when they undergo fracture under uniaxial tensile stress.

To gain deeper insight into the structural stability of confined water and its rupture behavior under tension, we analyzed the average lifetime of hydrogen bonds between water molecules in CNTs of various radius, as shown in Fig. 5. In

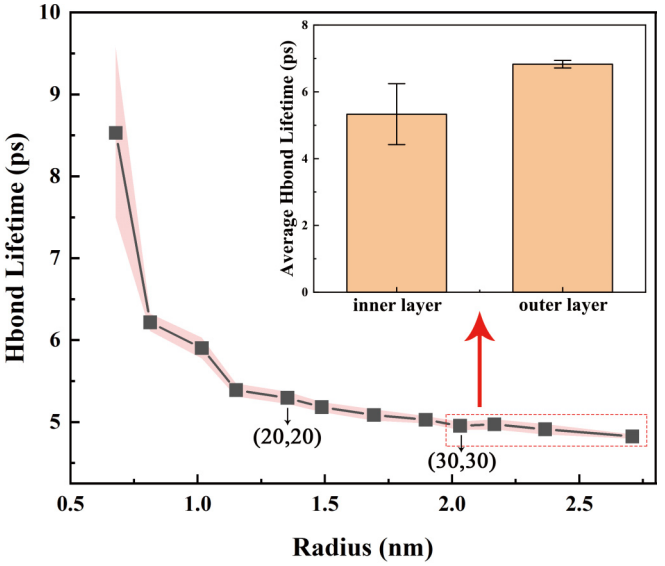


FIG. 5. Average lifetime of hydrogen bonds between water molecules confined in CNTs with different radius. The inset shows the hydrogen bond lifetimes between water molecules in the inner layer (i.e., the fourth water layer) and outer layers (i.e., the first, second, and third water layers), averaged over the (30,30) to (40,40) CNTs.

this study, hydrogen bonds were identified using a geometric criterion: a hydrogen bond is considered present when the distance between the oxygen atoms of two water molecules is less than 3.5 Å and the O···O–H angle is less than 30°. The hydrogen bond lifetime was calculated using the intermittent definition [50]. The results reveal two distinct regimes. When the $r \leqslant 1.353$ nm [corresponding to a (20,20) nanotube], the average hydrogen bond lifetime decreases sharply with increasing radius. For $r > 1.353$ nm, the decrease becomes more gradual, indicating reduced confinement effects on hydrogen bond dynamics. To elucidate the origin of rupture in large-diameter CNTs, where failure typically initiates at the center, we divided the confined water into an inner layer (the fourth water layer) and outer layers (first to third layers). The average hydrogen bond lifetime in the inner layer is approximately 5.3 ps, compared to 6.8 ps in the outer layers. The corresponding hydrogen bond energies are 11.7 kJ/mol and 17.0 kJ/mol, respectively. These results indicate that hydrogen bonds in the inner layer are weaker and less stable, which explains the preferential rupture initiation from the center under axial tension.

The ultrahigh tensile strength of water confined in carbon nanotubes is induced by the nanoconfinement effect, which arises from the synergistic action of strong hydrogen bonding between water molecules and intermolecular interactions between water and the carbon nanotube surfaces. These combined effects serve to stabilize water columns at the nanometer scale.

IV. CONCLUSIONS

In summary, we investigate the tensile behavior of water confined in CNTs with varying diameters via molecular dynamics simulations, aiming to shed light on the long-distance water transport mechanism in tall trees. We focus specifically on how spatial confinement affects the mechanical properties of the water columns, while neglecting other secondary factors. Carbon nanotubes serve as an ideal model system.

The tensile strength of confined water shows a distinct nonmonotonic dependence on CNT radius, peaking at ∼126 MPa when the tube radius is ∼1.35 nm. Structural analysis reveals that this dependence originates from the layered arrangement of water molecules inside CNTs: the tensile strength positively correlates with the number of ordered water layers and the maximum tensile strength coincides with the maximum number of discernible water layers (four layers) at $r =$ 1.35 nm. Beyond this radius, the expansion of the inner water layer weakens the structural stability, leading to a gradual decrease in tensile strength.

Fracture dynamic analysis indicates that confined water undergoes collective rupture of all layers when $r \leqslant 1.35$ nm, while an inside-out sequential rupture mode dominates for $r > 1.35$ nm. This difference is attributed to the weaker and less stable hydrogen bonds in the inner water layer compared to the outer layers. The ultrahigh tensile strength of confined water is ultimately ascribed to the synergistic effect of hydrogen bonding between water molecules and intermolecular interactions between water and CNT surfaces.

This work provides atomistic-level insights into the mechanical response of nanoconfined water, which not only deepens our understanding of the cohesion-tension theory for long-distance water transport in tall trees but also offers valuable guidance for the design of novel nanofluidic devices and biomimetic water transport systems.

DATA AVAILABILITY

The data that support the findings of this article are not publicly available upon publication because it is not technically feasible and/or the cost of preparing, depositing, and hosting the data would be prohibitive within the terms of this research project. The data are available from the authors upon reasonable request.

[1] G. Hummer, J. C. Rasaiah, and J. P. Noworyta, Water conduction through the hydrophobic channel of a carbon nanotube, Nature (London) **414**, 188 (2001).

[2] P. Kumar, S. V. Buldyrev, F. W. Starr, N. Giovambattista, and H. E. Stanley, Thermodynamics, structure, and dynamics of water confined between hydrophobic plates Phys. Rev. E **72**, 051503 (2005).

[3] H. Qiu and W. L. Guo, Electromelting of confined monolayer ice, Phys. Rev. Lett. **110**, 195701 (2013).

[4] Q. Yang, P. Sun, L. Fumagalli, Y. Stebunov, S. Haigh, Z. Zhou, I. Grigorieva, F. Wang, and A. Geim, Capillary condensation under atomic-scale confinement, Nature (London) **588**, 250 (2020).

[5] H. Lu, J. Li, X. Gong, R. Wan, L. Zeng, and H. Fang, Water permeation and wavelike density distributions inside narrow nanochannels, Phys. Rev. B **77**, 174115 (2008).

[6] R. P. Skelton, Quantifying plant hydraulic function becomes a tall order, J. Exp. Bot. **71**, 3927 (2020).

[7] S. Dasgupta, S. Saha, and F. Paesani, Reactivity of nanoconfined water is modulated by the properties of confining materials, J. Phys. Chem. Lett. **16**, 11996 (2025).

[8] F. Mei, X. Zhou, J. Kou, F. Wu, C. Wang, and H. Lu, A transition between bistable ice when coupling electric field and nanoconfinement, J. Chem. Phys. **142**, 134704 (2015).

[9] R. Zaleski, M. Gorgol, A. Kierys, P. Maheshwari, M. Pietrow, P. K. Pujari, and B. Zgardzińska, Unraveling the phase behavior of water confined in nanochannels through positron annihilation, J. Phys. Chem. C **126**, 5916 (2022).

[10] S. Q. He, M. Su, C. Tang, Y. F. Zheng, S. Y. Gao, H. Fang, and Y. Y. Zhang, Unique proton transfer and hydrogen evolution reaction at semi-disordered interfaces in confined spaces, J. Chem. Phys. **163**, 144708 (2025).

[11] F. Yang *et al.*, Controlling mass and energy diffusion with metamaterials, Rev. Mod. Phys. **96**, 015002 (2024).

[12] C. Duan, R. Karnik, M.-C. Lu, and A. Majumdar, Evaporation-induced cavitation in nanofluidic channels, Proc. Natl. Acad. Sci. USA **109**, 3688 (2012).

[13] S. Ghosh, A. Sood, and N. Kumar, Carbon nanotube flow sensors, Science **299**, 1042 (2003).

[14] J. K. Holt, H. G. Park, Y. M. Wang, M. Stadermann, A. B. Artyukhin, C. P. Grigoropoulos, A. Noy, and O. Bakajin, Fast mass transport through sub-2-nanometer carbon nanotubes, Science **312**, 1034 (2006).
[15] M. Whitby and N. Quirke, Fluid flow in carbon nanotubes and nanopipes, Nat. Nanotechnol. **2**, 87 (2007).
[16] Z. Zhu *et al.*, Covalent organic framework membranes from oppositely charged nanosheets toward efficient desalination, Small **20**, 2401172 (2024).
[17] S. Roman, F. Rembert, A. R. Kovscek, and J. Poonoosamy, Microfluidics for geosciences: Metrological developments and future challenges, Lab Chip **25**, 4273 (2025).
[18] K. Koga, X. C. Zeng, and H. Tanaka, Freezing of confined water: A bilayer ice phase in hydrophobic nanopores, Phys. Rev. Lett. **79**, 5262 (1997).
[19] K. Koga, G. T. Gao, H. Tanaka, and X. C. Zeng, Formation of ordered ice nanotubes inside carbon nanotubes, Nature (London) **412**, 802 (2001).
[20] C. Janiak, T. G. Scharmann, and S. A. Mason, Two-dimensional water and ice layers: Neutron diffraction studies at 278, 263, and 20 K, J. Am. Chem. Soc. **124**, 14010 (2002).
[21] R. Zangi and A. E. Mark, Monolayer ice, Phys. Rev. Lett. **91**, 025502 (2003).
[22] D. Takaiwa, I. Hatano, K. Koga, and H. Tanaka, Phase diagram of water in carbon nanotubes, Proc. Natl. Acad. Sci. USA **105**, 39 (2008).
[23] F. Mikami, K. Matsuda, H. Kataura, and Y. Maniwa, Dielectric properties of water inside single-walled carbon nanotubes, ACS Nano **3**, 1279 (2009).
[24] S. Han, M. Choi, P. Kumar, and H. E. Stanley, Phase transitions in confined water nanofilms, Nat. Phys. **6**, 685 (2010).
[25] Z. Fu, Y. Luo, J. Ma, and G. Wei, Phase transition of nanotube-confined water driven by electric field, J. Chem. Phys. **134**, 154507 (2011).
[26] Z. Qian and G. Wei, Electric-field-induced phase transition of confined water nanofilms between two graphene sheets, J. Phys. Chem. A **118**, 8922 (2014).
[27] W. Zhao, J. Bai, L.-F. Yuan, J. Yang, and X. C. Zeng, Ferroelectric hexagonal and rhombic monolayer ice phases, Chem. Sci. **5**, 1757 (2014).
[28] X. Zhu, Q. Yuan, and Y.-P. Zhao, Phase transitions of a water overlayer on charged graphene: From electromelting to electrofreezing, Nanoscale **6**, 5432 (2014).
[29] J. Chen, G. Schusteritsch, C. J. Pickard, C. G. Salzmann, and A. Michaelides, Two dimensional ice from first principles: Structures and phase transitions, Phys. Rev. Lett. **116**, 025501 (2016).
[30] J. Jiang, Y. Gao, W. Zhu, Y. Liu, C. Zhu, J. S. Francisco, and X. C. Zeng, First-principles molecular dynamics simulations of the spontaneous freezing transition of 2D water in a nanoslit, J. Am. Chem. Soc. **143**, 8177 (2021).
[31] W. Zhao, H. Qiu, and W. Guo, A deep neural network potential for water confined in graphene nanocapillaries, J. Phys. Chem. C **126**, 10546 (2022).
[32] S. Joseph and N. R. Aluru, Why are carbon nanotubes fast transporters of water? Nano Lett. **8**, 452 (2008).
[33] K. Falk, F. Sedlmeier, L. Joly, R. R. Netz, and L. Bocquet, Molecular origin of fast water transport in carbon nanotube membranes: Superlubricity versus curvature dependent friction, Nano Lett. **10**, 4067 (2010).
[34] Q.-L. Zhang, W.-Z. Jiang, J. Liu, R.-D. Miao, and N. Sheng, Water transport through carbon nanotubes with the radial breathing mode, Phys. Rev. Lett. **110**, 254501 (2013).
[35] J. Kou, H. Lu, F. Wu, J. Fan, and J. Yao, Electricity resonance-induced fast transport of water through nanochannels, Nano Lett. **14**, 4931 (2014).
[36] M. Majumder, N. Chopra, R. Andrews, and B. J. Hinds, Erratum: Nanoscale hydrodynamics: Enhanced flow in carbon nanotubes, Nature (London) **438**, 930 (2005).
[37] Q. Xie, M. A. Alibakhshi, S. Jiao, Z. Xu, M. Hempel, J. Kong, H. G. Park, and C. Duan, Fast water transport in graphene nanofluidic channels, Nat. Nanotechnol. **13**, 238 (2018).
[38] D. Becerra, A. Córdoba, J. H. Walther, and H. A. Zambrano, Water flow in a polymeric nanoslit channel with graphene and hexagonal boron nitride wall coatings: An atomistic study, Phys. Fluids **35**, 14 (2023).
[39] B. Radha *et al.*, Molecular transport through capillaries made with atomic-scale precision, Nature (London) **538**, 222 (2016).
[40] M. Wu, W. Wei, X. Liu, K. Liu, and S. Li, Structure and dynamic properties of stretched water in graphene nanochannels by molecular dynamics simulation: Effects of stretching extent, Phys. Chem. Chem. Phys. **21**, 19163 (2019).
[41] G. Algara-Siller, O. Lehtinen, F. C. Wang, R. R. Nair, U. Kaiser, H. A. Wu, A. K. Geim, and I. V. Grigorieva, Square ice in graphene nanocapillaries, Nature (London) **519**, 443 (2015).
[42] M. Masuduzzaman, C. Bakli, M. Barisik, and B. Kim, Anomalous water flow in sub-nanometer carbon nanoconfinement, Small **21**, e08637 (2025).
[43] M. T. Tyree, Plant hydraulics: The ascent of water, Nature (London) **423**, 923 (2003).
[44] F. W. Bentrup, Water ascent in trees and lianas: The cohesion-tension theory revisited in the wake of Otto Renner, Protoplasma **254**, 627 (2017).
[45] C. Wei, M. T. Tyree, and E. Steudle, Direct measurement of xylem pressure in leaves of intact maize plants. A test of the cohesion-tension theory taking hydraulic architecture into consideration, Plant Physiol. **121**, 1191 (1999).
[46] S. J. Lee, H. Kim, and S. Ahn, Water transport in porous hydrogel structures analogous to leaf mesophyll cells, Microfluid. Nanofluid. **18**, 775 (2014).
[47] J. Shi and S. Avramidis, Evolution of wood cell wall nanopore size distribution in the hygroscopic range, Holzforschung **73**, 899 (2019).
[48] A. Srivastava, J. Hassan, and D. Homouz, Effect of size and temperature on water dynamics inside carbon nano-tubes studied by molecular dynamics simulation, Molecules **26**, 6175 (2021).
[49] A. Alexiadis and S. Kassinos, Molecular simulation of water in carbon nanotubes, Chem. Rev. **108**, 5014 (2008).
[50] M. Antipova and V. Petrenko, Hydrogen bond lifetime for water in classic and quantum molecular dynamics, Russ. J. Phys. Chem. A **87**, 1170 (2013).